Computational mechanistic studies of the carbon-carbon double bond difunctionalization via epoxidation and subsequent aminolysis in vegetable oils

Yusif Abdullayev*[a,b], Vaqif Abbasov[b], Fizuli Nasirov[b], Nigar Rzayeva[b], Leyla Nasibova[c], Jochen Autschbach*[d]

[a] Department of Chemical Engineering, Baku Engineering University, Hasan Aliyev str. 120, Baku, Absheron, AZ0101, Azerbaijan. Email: yabdullayev@beu.edu.az

[b] Institute of Petrochemical Processes, Azerbaijan National Academy of Sciences, Baku AZ1025, Azerbaijan

[c] Department of Chemistry, Ganja State University, Heydar Aliyev Ave 425, AZ2001, Ganja, Azerbaijan

[d] Department of Chemistry, University at Buffalo, State University of New York, Buffalo, New York 14260-3000, United States. Email: jochena@buffalo.edu

Keywords: C=C double bond, DFT, catalyst, epoxide ring-opening, energetic span

Abstract: The industrial importance of the C=C double bond difunctionalization in vegetable oils/fatty acid chains motivates computational studies aimed at helping to improve experimental protocols. The C=C double bond epoxidation is studied with hydrogen peroxide, peracetic acid (CH_3CO_3H), and performic acid (HCO_3H) oxidizing agents. The epoxide ring-opening mechanism is calculated in the presence of $ZnCl_2$, $NiCl_2$, and $FeCl_2$ Lewis acidic catalysts. Computations show that H_2O_2 ($\Delta G^{\ddagger}$=39 kcal/mol, **TS1$_{HP}$**) is not an effective oxidizing agent compared to CH_3CO_3H ($\Delta G^{\ddagger}$=29.8 kcal/mol, **TS1$_{PA}$**) and HCO_3H ($\Delta G^{\ddagger}$=26.7 kcal/mol, **TS1$_{PF}$**). The $FeCl_2$ ($\Delta G^{\ddagger}$=14.7 kcal/mol, **TS1$_{FC}$**) coordination to the epoxide oxygen facilitates the ring-opening via lower energy barriers compared to the $ZnCl_2$ ($\Delta G^{\ddagger}$=19.5 kcal/mol, **TS1$_{ZC}$**) and $NiCl_2$ ($\Delta G^{\ddagger}$=29.4 kcal/mol, **TS1$_{NC}$**) coordination. $ZnCl_2$ was frequently utilized as a catalyst in laboratory-scale procedures. The energetic span model identifies the $FeCl_2$ (FC) catalytic cycle as the best option for the epoxide ring-opening.

1. Introduction

The C=C double bond is very important in synthetic applications because of its reactivity[1]. C=C bond bearing compounds can act as building blocks for several functionalities such as amines, alcohols, aldehydes, epoxides, or acids[2-4]. Naturally available and low-cost C=C bond containing substances can act as an alternative to fossil fuels: Among vegetable oils, soybean oil, in particular, contains roughly 60 wt% linoleic acid, and a total of 80 wt% unsaturated residues, which makes it more modifiable and eventually

more applicable compared to other vegetable oils. The unsaturated fatty acids have been functionalized to the polyols, mercapto components, epoxides, copolymers, and homopolymers[5,6]. These substances are utilized as fuel additives, biodiesel, and biolubricants[7,8]. Modification of waste vegetable oil plays a crucial role in the industry as a sustainable substitute for fossil-based resources[9,10]. The epoxy ring-opening with amines led to the formation of nitrogen-based triglyceride formation, which was utilized as lubricant additives[11,12]. These products are antiwear/antifriction additives for industrial oils and automotive applications. Kinetic studies have been performed for aminolysis of carbonated vegetable oils to polyurethanes[13,14].

The conversion of abundant unsaturated triglyceride to value-added components is crucial because of the sustainability point of view. The applications mentioned above inspire us to perform mechanistic studies on the double bond transformation to epoxides and the nucleophilic (amine) epoxide ring-opening (Scheme 1). Due to the importance of the double bond modifications, extensive computational studies with a related scope have been performed so far[15-19]. But none of these works comparatively studied experimentally employed oxidizing agents. Computational tools were applied previously for the understanding of reaction mechanisms[20-27]. We chose a model reaction to reduce computational time for the present mechanistic studies: Instead of macromolecular triglyceride, but-2-ene was taken as the internal double bond carrier. Since the macromolecular triglycerides have very flexible structures, we do not expect the reaction pathways to be influenced strongly by steric bulk. Hydrogen peroxide (H_2O_2, **HP**), peracetic acid (CH_3CO_3H, **PA**), and performic acid (HCO_3H, **PF**) were utilized as oxidizing agents. For the nucleophilic epoxide ring-opening, Lewis acidic catalysts ($ZnCl_2$, $NiCl_2$, and $FeCl_2$) and ethylamine (nucleophile) were examined. The free energy surface was recalculated in the presence of oleic acid (one of the tails of soybean oil) for epoxidation and epoxide ring-opening steps to validate the simplification. In the case of oleic acid, 1 kcal decrease in the epoxidation ($\mathbf{TS_{PF}}$) energy barrier is noticed compared to the but-2-ene incorporated **PF** route. For the **HP** and **PA** steps, the energy barriers decrease even smaller than 1 kcal. Based on the theory, the model reaction (with but-2-ene) can be exploited computationally to simplify fatty acid esters epoxidation and consequent epoxide ring-opening reactions (See SI, Figures S4, S5; Tables S6, S7).

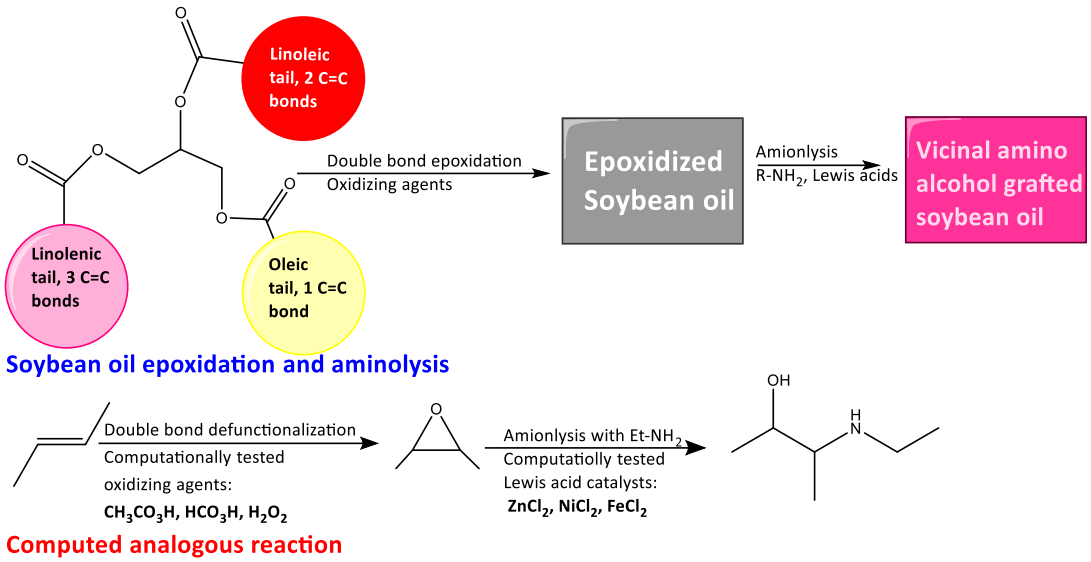

Scheme 1. The unsaturated fatty acids triglyceride conversion to the lubricant precursors.

2. Computational details.

The Gaussian 16 software package[28] was used for all calculations. Reactants, intermediates, and transition state structures were fully optimized with Kohn-Sham Density Functional Theory (KS-DFT), employing the B3LYP functional[29]. Minnesota functionals (M06L and M062X) were also applied to re-evaluate the best catalytic cycle ($FeCl_2$) of Figure 2 because of these functionals' demonstrated accuracy in energy barrier evaluations[30]. The B3LYP functional with D3BJ dispersion corrections was also tested for the $FeCl_2$ catalyzed oxirane ring-opening (See Figure S1, SI). Computation shows that there are no considerable changes in the energy barriers, and the B3LYP functional is reliable for the studied reaction. The 6-311+G* basis set was used for H, C, O, N, and Cl atoms. The Stuttgart 1997 RSC effective core potentials (ECP) and matching basis sets were used for Zn, Ni, and Fe[31,32].

Because of the Ni^{2+} and Fe^{2+} paramagnetic nature, we monitored the NC and FC catalytic cycles Gibbs energies for singlet and triplet spin states. The linear $NiCl_2$ molecule adopts a triplet spin state, and consequently, the NC catalytic cycle was calculated for the spin-triplet potential energy surface (PES). A spin state change during the reaction would constitute a spin-forbidden reaction step in an otherwise already very fast reaction (vide infra). The molecular orbital (MO) analysis shows that one of the unpaired orbital interacts with organic system in the $\mathbf{TS1_{NC}}$ and $\mathbf{TS2_{NC}}$ structures (See Figure S2 and S3, SI). DFT calculations with different functionals for $FeCl_2$ produced a spin-triplet ground state, but with severe spin contamination. The molecule has two electrons less than $NiCl_2$ and should therefore adopt a spin-singlet closed-shell ground state. Indeed, optimizations with simultaneous monitoring of the wavefunction

stability eventually produced the singlet as the ground spin state of $FeCl_2$, with a slightly bent optimized structure. We tentatively attribute the severe spin symmetry breaking in the triplet and the slight spatial symmetry breaking in the singlet to difficulties that the DFT calculations have in treating the electron correlation in this molecule. The FC catalytic cycle was calculated for the spin-singlet PES. Solvent effects were studied via a self-consistent reaction field (SCRF) with a dielectric constant for n-hexane (ε=1.8819) for the **PF** oxidation route and the FC catalytic cycle. Minima (no imaginary frequency), transition states (one imaginary frequency), and free energies (including entropy contributions from rotations, vibrations, and translation) were determined via analytic frequency calculations. Gibbs energies and related data are given for a temperature of 298.15 K because of experimentally applied procedures[33,34]. Intrinsic reaction coordinate (IRC) searches were applied to connect the transition state (TS) and intermediate/product structures. Total energies, Gibbs energies, and enthalpies of all structures are given in the supporting information (SI).

3. Results and discussion

Effective epoxidation of vegetable oils is one of the challenging processes that determines the efficiency of the next step treatment, i.e., hydroxylation, N-alkylation, and O-alkylation[35-38].

Figure 1 shows **HP**, **PA**, and **PF** mediated epoxidation routes. **HP** was employed previously as an oxidizing agent in vegetable oil epoxidation processes[8,33,39]. The computations show that **HP** is not an effective oxidizing agent for epoxidation due to the high energy barrier (39 kcal/mol). The **HP** week oxidation abilities were

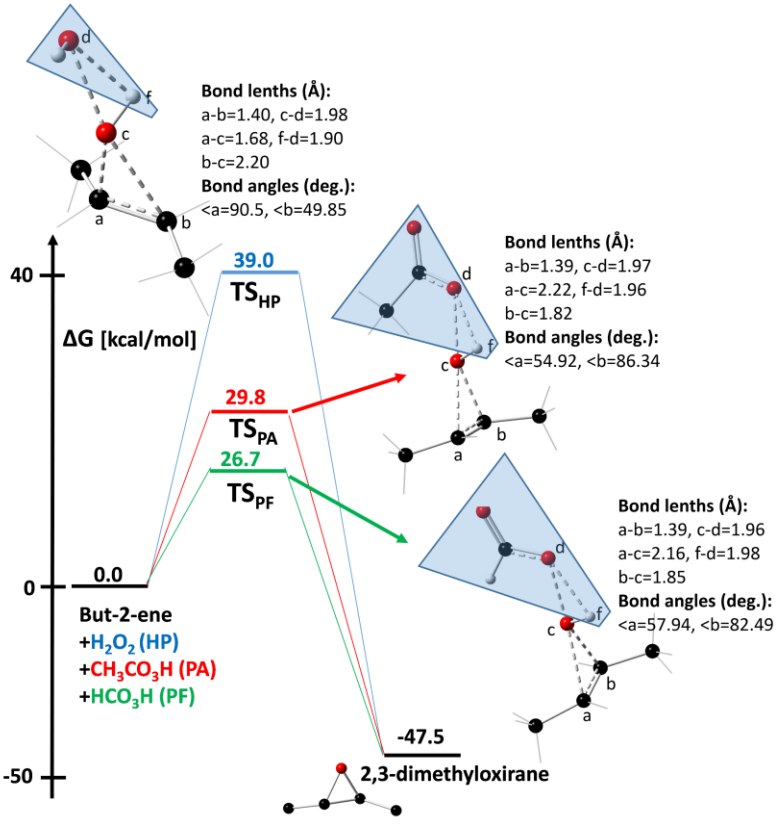

Figure 1. Free energy profile for the epoxidation of but-2-ene. Blue, red, and green colors correspond to the **HP**, **PA**, and **PF** employed routes. In the TS structures the but-2-ene hydrogens are omitted to avoid clutter. The blue shaded areas indicate leaving molecules (H_2O, HCOOH, and CH_3COOH) after oxidation.

scrutinized in experimental studies with less solubility in organic phase[40].

In comparison, the **PA** and **PF** activation energies are 9.2 kcal/mol and 12.3 kcal/mol lower, respectively. Since **PF** gave the reaction with the lowest barrier (26.7 kcal/mol) the reaction was recalculated, including the solvation model for n-hexane. Investigations show that the **PF** route activation energy is decreased by 4 kcal/mol compared to the gas-phase condition. We focus here on the gas-phase reaction profiles because of experimentally employed solvent-free epoxidation conditions for the unsaturated fatty acid esters[41,42]. Computation shows that the application of solvent may not be a driving force for the epoxidation process, but it is very vital for the epoxide ring-opening. The utilization of a solvent helps to decrease the vegetable oil viscosity and a reaction time[5]. Structural analysis of the TSs illustrates that oxygen migration from **HP** to the double bond carrier occurs over shorter distances ($\mathbf{TS_{HP}}$, 1.68 Å) compared to the **PA** ($\mathbf{TS_{PA}}$, 1.82 Å) and **PF** ($\mathbf{TS_{PF}}$, 1.85 Å). While at the same time, there is more elongation of the double bond, leading to the comparatively high energy of $\mathbf{TS_{HP}}$. Because of the **PF** instability, *in situ* generation of **PF** via using formic acid and hydrogen peroxide was applied in the past works[35,43]. Kinetic studies showed that **PF** decomposition occurs at a high temperature[44]. Previous experimental works proposed **PF** as a better oxidizing agent to carry out the vegetable oil epoxidation (with 97% conversion[45]) and are in good agreement with our computational studies.

Epoxide ring-opening: The epoxide ring-opening was initially calculated in a catalyst-free condition (Figure 2). Concerted $\mathbf{TS_{CAT\_FREE}}$ is obtained for the one-step direct transformation of $EtNH_2$ and 2,3-methyloxirane to 3-(ethylamino)butan-2-ol (**PRO**) via 54.2 kcal/mol energy barrier. A similar energy barrier was calculated previously for the epoxide ring-opening in catalyst-free condition[46]. The calculated energy barrier shows that utilizing a catalyst will be a cost-effective option for the process. Because of the extensive application of Lewis acid catalysis in the aminolysis of epoxides to β-amino alcohols[47,48], we chose $ZnCl_2$, $NiCl_2$, and $FeCl_2$ for the calculations. In particular, aminolysis of the epoxidized unsaturated fatty esters has been carried out with $ZnCl_2$[49-52]. As seen from Figure 2, the Lewis acid coordination and Et_2NH_2 nucleophilic attack go through a concerted TS (**TS1**). It can be considered the rate-limiting step for all three reaction routes (ZC, NC, FC). In the case of the $ZnCl_2$ catalyzed cycle, the ring-opening energy barrier is calculated to be 19.5 kcal/mol (relative to $\mathbf{IM1_{ZC}}$). The analogous barrier is found to be 29.4 kcal/mol and 14.7 kcal/mol for the $NiCl_2$ and $FeCl_2$ routes, respectively. We recalculated FC including solvent effects (solvent: n-Hexane) and observed only small changes (less than 3 kcal) in the energy barriers. Calculations show a little difference in bond distances when comparing the n-hexane included $\mathbf{TS2_{FC}}$ with the solvent-free version (see Figure 3). The solvent incorporation causes the N-H bond to

elongate from 1.28 Å to 1.31 Å, and the H-O bond becomes shorter (from 1.25 Å to 1.21 Å). The fact implies that the addition of solvent facilitates proton transfer from the amine group to the epoxide oxygen. Since activation energies alone are insufficient to assess catalytic cycles, we employed an energetic span (δG) model for computational TOF (turnover frequency) calculations[53]. As seen from the Gibbs energy profiles, the lowest energy TOF determining intermediate (**IM2**, TDI) appears after **TS1** (the highest energetic TOF determining TS, TDTS), which directed us to use Eq. [2][25]:

$$TOF = \frac{k_B T}{h} e^{\frac{-\delta G}{RT}} \quad \textbf{Eq. [1]}$$

$$\delta G = G_{TDTS} - G_{TDI} + G_r \quad \textbf{Eq. [2]}$$

Catalytic Cycles	δG (kcal/mol)
ZC (blue, $ZnCl_2$)	7.9
NC (orange, $NiCl_2$)	14.5
FC (grey, $FeCl_2$)	-28.7

Table 1. Calculated δG values for the catalytic cycles.

k_B stands for Boltzmann constant, h is Plank constant, R is universal gas constant, T is temperature in Kelvin, and G_r is the reaction Gibbs energy. The G_r value is different for each route because **PRO$_{FC}$**, **PRO$_{NC}$**, and **PRO$_{ZC}$** structures include the product and the corresponding Lewis acid catalyst. The catalyst metal and the product heteroatoms (N, O) undergo electrostatic interactions that differentiate the product energies, which is not contradictory to the chemical kinetic law. Table 1 shows δG for the catalytic cycles derived from Eq. [2]. Theoretical TOF values are calculated based on the Eyring equation (See Eq. [1] and Table S5). $FeCl_2$ emerges as a better suitable

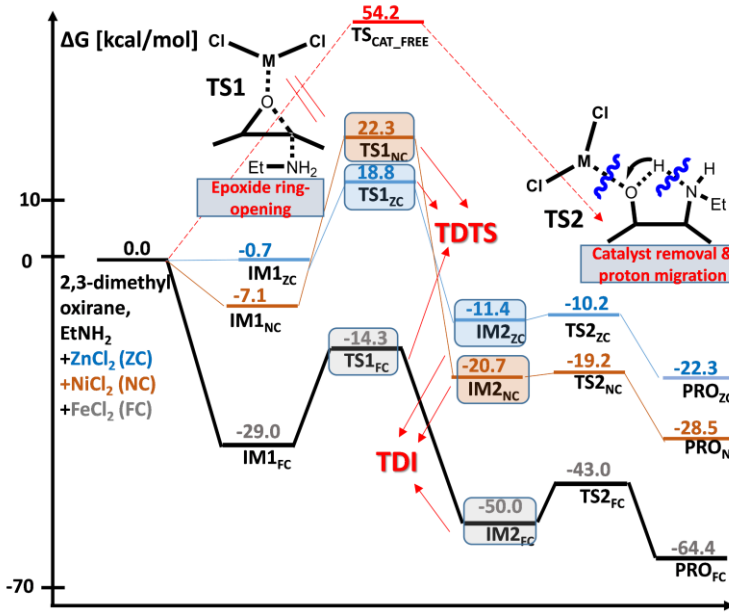

Figure 2. Gibbs energy profile for the oxirane ring opening in the catalyst-free and catalytic conditions. Red: catalyst-free, orange: $NiCl_2$, blue: $ZnCl_2$, black: $FeCl_2$ promoted catalytic routes. Singlet spin state Gibbs energies are reported for the ZC and FC catalytic cycles. Since triplet spin state is determined as a ground state for NC, related Gibbs energies are included to the energy profile.

catalyst for the epoxide ring-opening compared to the other two candidates. $\frac{TOF_{FC}}{TOF_{ZC}} = 10^{26}$ demonstrates that 20.8 kcal decrease in the δG value (from ZC to FC) leads to a huge rise in the theoretical catalytic efficiency (TOF). In fact, the calculated TOFs for ZC, and in particular for FC, should not be considered as physical TOFs. They are simply large enough to indicate that the reaction rate in the catalyzed process is likely not limited by features of the Gibbs energy profile intrinsic to the reaction, but rather by the dynamics of the reaction system under the experimental conditions. Nonetheless, the calculations provide strong indications that $FeCl_2$ will be a superior catalyst for the epoxide ring-opening reaction. Experimental utilization of magnetite (Fe_3O_4) for the regioselective epoxide ring-opening and $FeCl_3$ catalyzed Friedel-Crafts reaction accompanied ring-opening of 1,4-epoxy moieties were previously reported[54,55].

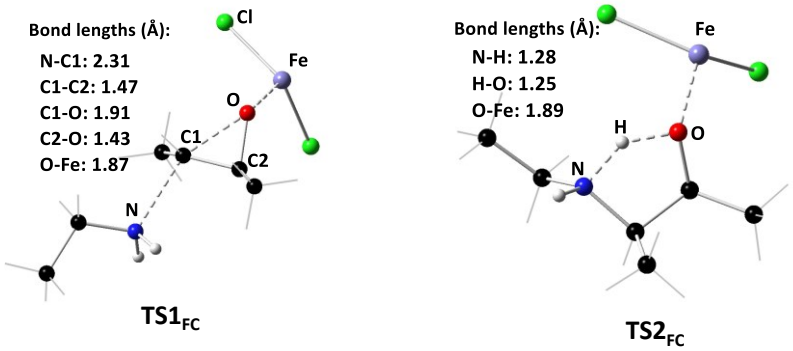

Figure 3. Optimized TS structures for the epoxide ring-opening (**TS1$_{FC}$**) and the amine proton transfer to the epoxide oxygen (hydroxylation, **TS2$_{FC}$**). Some hydrogen atoms are omitted for the sake of clarity.

The optimized structures of the **TS1$_{FC}$** and **TS2$_{FC}$** are shown in Figure 3. As seen from the Figure, the $EtNH_2$ nucleophilic attack occurs via 2.31 Å separation between **N** and **C1** in the transition state, while the **C1-O** bond elongates up to 1.91 Å in the concerted **TS1$_{FC}$** structure. The amine moiety proton transfers to the epoxide oxygen via 1.27 Å (**N-H**) and 1.25 Å (**H-O**) bond lengths (Figure 3, **TS2$_{FC}$**). Since the reaction rate depends on the first TS, we conducted a natural bond orbital (NBO) analysis to determine natural charges of all atoms in the **TS1$_{FC}$** structure. Heterolytic **C1-O** bond cleavage results in the accumulation of electron density on the **O** atom. The accumulated density is delocalized well in the case of $FeCl_2$ coordination: In the original epoxide ring, the oxygen charge is -0.57 *e*; upon coordination with **Fe** it becomes -0.66 *e* in the **TS1$_{FC}$** structure. The epoxide oxygen atom is expected to be more electronegative because of **C1→O** electron shift. The small change in the epoxide oxygen natural charge indicates the electron follows

toward the catalyst ($FeCl_2$). Natural charge decreases in **Fe** (0.69 *e* to 0.65 *e*) and **Cl** (-0.33 *e* to -0.49 *e*) (relative to sole $FeCl_2$ molecule[56] natural charges) shows electron shift toward $FeCl_2$. NBO analysis is applied to the same TS from the high energy catalytic cycle (ZC): In the case of $ZnCl_2$ coordination, high electron density (less delocalization) is observed on the epoxide oxygen (-0.85 *e*, which is -0.66 in the $FeCl_2$ case, **$TS1_{FC}$**). $ZnCl_2$ is not capable of withdrawing electron density as well as $FeCl_2$ to facilitate the ring-opening. $FeCl_2$ superior catalytic activities for the epoxide ring-opening can be rationalized with better electron delocalization upon coordinating to the epoxide ring oxygen.

4. Conclusions

The carbon-carbon double bond difunctionalization through epoxidation and the subsequent epoxide ring aminolysis was studied computationally. The H_3CO_3H (**PF**) energy barrier was found to be smaller ($\Delta G^{\ddagger}$=26.7 kcal/mol, **$TS1_{PF}$**) than the other two oxidation routes (Figure 1). The epoxide ring-opening was studied with three Lewis acid catalysts ($ZnCl_2$, $NiCl_2$, and $FeCl_2$). The rate-limiting energy barrier for the FC cycle was found to be 3.4 kcal less than in the ZC cycle. Despite the regular utilization of $ZnCl_2$ in practice, our computations suggest that $FeCl_2$ would be a better catalyst, based on the applied energetic span model. Since iron is an inexpensive metal, we hope that the present calculations will motivate experimental verification of this prediction. We believe this work will contribute to the waste vegetable oils cost-effective industrial utilization.

Conflicts of interest

There are no conflicts to declare

Acknowledgments

Y.A. acknowledges the financial support from the BP Azerbaijan (grant-CW2192142) and the SOCAR Science Foundation, S/N 17LR-AMEA (10 September 2019). The authors thank the Center for Computational Research (CCR) at the University at Buffalo for providing computational resources. JA acknowledges support from grant CHE-1855740 from the National Science Foundation.

References

1. Liu, Y.-Y.; Yang, X.-H.; Song, R.-J.; Luo, S.; Li, J.-H. Nature Communications 2017, 8(1), 14720.
2. Li, Y.; Wu, D.; Cheng, H.-G.; Yin, G. Angewandte Chemie International Edition 2020, 59(21), 7990-8003.
3. Romero, R. M.; Wöste, T. H.; Muñiz, K. Chem. - Asian J. 2014, 9(4), 972-983.
4. Cardona, F.; Goti, A. Nature Chemistry 2009, 1(4), 269-275.

5. Desroches, M.; Caillol, S.; Lapinte, V.; Auvergne, R.; Boutevin, B. Macromolecules 2011, 44(8), 2489-2500.
6. Karmakar, G.; Ghosh, P. ACS Sustainable Chemistry & Engineering 2015, 3(1), 19-25.
7. Santos, E. M.; Piovesan, N. D.; de Barros, E. G.; Moreira, M. A. Fuel 2013, 104, 861-864.
8. Karmakar, G.; Ghosh, P.; Sharma, K. B. Lubricants 2017, 5(4).
9. Dey, P.; Ray, S. Clean Technologies and Environmental Policy 2020, 22(7), 1517-1530.
10. Naeem, M. M.; Al-Sakkari, E. G.; Boffito, D. C.; Gadalla, M. A.; Ashour, F. H. Fuel 2021, 283, 118914.
11. Schuchardt, K. L.; Didier, B. T.; Elsethagen, T.; Sun, L.; Gurumoorthi, V.; Chase, J.; Li, J.; Windus, T. L. J. Chem. Inf. Model. 2007, 47(3), 1045-1052.
12. Atanu Biswas, K. M. D., Huai Nan Cheng, Brajendra K. Sharma. In US8841470B1; Penn State Research Foundation, U. D. o. A., Ed.: US, 2011.
13. Guzmán Agudelo, A. F.; Pérez-Sena, W. Y.; Kebir, N.; Salmi, T.; Ríos, L. A.; Leveneur, S. Chemical Engineering Science 2020, 228, 115954.
14. Pérez-Sena, W. Y.; Cai, X.; Kebir, N.; Vernières-Hassimi, L.; Serra, C.; Salmi, T.; Leveneur, S. Chemical Engineering Journal 2018, 346, 271-280.
15. Kakiuchi, F. In The Directed Metallation; Chatani, N., Ed.; Springer Berlin Heidelberg: Berlin, Heidelberg, 2007, p 1-33.
16. Liu, L.; Pei, G.; Liu, P.; Ling, B.; Liu, Y.; Bi, S. J. Org. Chem. 2018, 83(4), 2067-2076.
17. Bach, R. D.; Glukhovtsev, M. N.; Gonzalez, C.; Marquez, M.; Estévez, C. M.; Baboul, A. G.; Schlegel, H. B. The Journal of Physical Chemistry A 1997, 101(34), 6092-6100.
18. Lundin, A.; Panas, I.; Ahlberg, E. The Journal of Physical Chemistry A 2009, 113(1), 282-290.
19. Bach, R. D.; Canepa, C.; Winter, J. E.; Blanchette, P. E. The Journal of Organic Chemistry 1997, 62(15), 5191-5197.
20. Abdullayev, Y.; Mammadov, A.; Karimova, N.; Talybov, A.; Yolchuyeva, U.; Autschbach, J. ChemistrySelect 2020, 5(20), 6224-6229.
21. Li, Z.; Boyarskikh, V.; Hansen, J. H.; Autschbach, J.; Musaev, D. G.; Davies, H. M. L. J. Am. Chem. Soc. 2012, 134(37), 15497-15504.
22. Valiyev, I.; Abdullayev, Y.; Yagubova, S.; Baybekov, S.; Salmanov, C.; Autschbach, J. J. Mol. Liq. 2019, 280, 410-419.
23. Abdullayev, Y.; Sudjaev, A.; Autschbach, J. J. Mol. Model. 2019, 25(6), 173.
24. Contreras, R. H.; Llorente, T.; Ducati, L. C.; Tormena, C. F. J. Phys. Chem. A 2014, 118(27), 5068-5075.
25. Abdullayev, Y.; Abbasov, V.; Ducati, L. C.; Talybov, A.; Autschbach, J. ChemistryOpen 2016, 5(5), 460-469.
26. Dyduch, K.; Srebro-Hooper, M.; Lee, B. Y.; Michalak, A. J. Comput. Chem. 2018, 39(23), 1854-1867.
27. Wolters, L. P.; Bickelhaupt, F. M. Chem. - Asian J. 2015, 10(10), 2299-2299.
28. Frisch, M. J.; Trucks, G. W.; Schlegel, H. B.; Scuseria, G. E.; Robb, M. A.; Cheeseman, J. R.; Scalmani, G.; Barone, V.; Petersson, G. A.; Nakatsuji, H.; Li, X.; Caricato, M.; Marenich, A. V.; Bloino, J.; Janesko, B. G.; Gomperts, R.; Mennucci, B.; Hratchian, H. P.; Ortiz, J. V.; Izmaylov, A. F.; Sonnenberg, J. L.; Williams; Ding, F.; Lipparini, F.; Egidi, F.; Goings, J.; Peng, B.; Petrone, A.; Henderson, T.; Ranasinghe, D.; Zakrzewski, V. G.; Gao, J.; Rega, N.; Zheng, G.; Liang, W.; Hada, M.; Ehara, M.; Toyota, K.; Fukuda, R.; Hasegawa, J.; Ishida, M.; Nakajima, T.; Honda, Y.; Kitao, O.; Nakai, H.; Vreven, T.; Throssell, K.; Montgomery Jr., J. A.; Peralta, J. E.; Ogliaro, F.; Bearpark, M. J.; Heyd, J. J.; Brothers, E. N.; Kudin, K. N.; Staroverov, V. N.; Keith, T. A.; Kobayashi, R.; Normand, J.; Raghavachari, K.; Rendell, A. P.; Burant, J. C.; Iyengar, S. S.; Tomasi, J.; Cossi, M.; Millam, J. M.; Klene, M.; Adamo, C.; Cammi, R.; Ochterski, J. W.; Martin, R. L.; Morokuma, K.; Farkas, O.; Foresman, J. B.; Fox, D. J.; Gaussian Inc. Wallingford CT, 2016.
29. Hehre, W. J.; Ditchfield, R.; Pople, J. A. J. Chem. Phys. 1972, 56(5), 2257-2261.

30. Mardirossian, N.; Head-Gordon, M. Journal of Chemical Theory and Computation 2016, 12(9), 4303-4325.
31. Martin, J. M. L.; Sundermann, A. J. Chem. Phys. 2001, 114(8), 3408-3420.
32. Dolg, M.; Wedig, U.; Stoll, H.; Preuss, H. J. Chem. Phys. 1987, 86(2), 866-872.
33. Plaza, D. D.; Strobel, V.; Heer, P. K. K. S.; Sellars, A. B.; Hoong, S.-S.; Clark, A. J.; Lapkin, A. A. J. Chem. Technol. Biotechnol. 2017, 92(9), 2254-2266.
34. Harry-O'kuru, R. E.; Tisserat, B.; Gordon, S. H.; Gravett, A. J. Agric. Food Chem. 2015, 63(29), 6588-6595.
35. Campanella, A.; Fontanini, C.; Baltanás, M. A. Chemical Engineering Journal 2008, 144(3), 466-475.
36. Cai, X.; Zheng, J. L.; Aguilera, A. F.; Vernières-Hassimi, L.; Tolvanen, P.; Salmi, T.; Leveneur, S. International Journal of Chemical Kinetics 2018, 50(10), 726-741.
37. Prileschajew, N. Berichte der deutschen chemischen Gesellschaft 1909, 42(4), 4811-4815.
38. Wisniak, J.; Navarrete, E. Product R&D 1970, 9(1), 33-41.
39. Santacesaria, E.; Tesser, R.; Di Serio, M.; Turco, R.; Russo, V.; Verde, D. Chemical Engineering Journal 2011, 173(1), 198-209.
40. Rangarajan, B.; Havey, A.; Grulke, E. A.; Culnan, P. D. Journal of the American Oil Chemists' Society 1995, 72(10), 1161-1169.
41. Cai, S.; Wang, L. Chin. J. Chem. Eng. 2011, 19(1), 57-63.
42. Wei, Y.; Li, G.; Lv, Q.; Cheng, C.; Guo, H. Ind. Eng. Chem. Res. 2018, 57(48), 16284-16294.
43. Zheng, J. L.; Wärnå, J.; Salmi, T.; Burel, F.; Taouk, B.; Leveneur, S. AIChE Journal 2016, 62(3), 726-741.
44. Leveneur, S.; Thönes, M.; Hébert, J.-P.; Taouk, B.; Salmi, T. Ind. Eng. Chem. Res. 2012, 51(43), 13999-14007.
45. Cai, X.; Matos, M.; Leveneur, S. Ind. Eng. Chem. Res. 2019, 58(4), 1548-1560.
46. Asadov, Z. H.; Ahmadova, G. A.; Rahimov, R. A.; Hashimzade, S.-Z. F.; Abdullayev, Y.; Ismailov, E. H.; Suleymanova, S. A.; Asadova, N. Z.; Zubkov, F. I.; Autschbach, J. J. Mol. Liq. 2020, 302, 112579.
47. Mai, E.; Schneider, C. Chem. - Eur. J. 2007, 13(9), 2729-2741.
48. Singh, M. C.; Peddinti, R. K. Tetrahedron Lett. 2007, 48(41), 7354-7357.
49. Biswas, A.; Adhvaryu, A.; Gordon, S. H.; Erhan, S. Z.; Willett, J. L. J. Agric. Food. Chem. 2005, 53(24), 9485-9490.
50. Mąka, H.; Spychaj, T.; Adamus, J. R. Soc. Chem. Adv. 2015, 5(101), 82813-82821.
51. Durán Pachón, L.; Gamez, P.; van Brussel, J. J. M.; Reedijk, J. Tetrahedron Lett. 2003, 44(32), 6025-6027.
52. Ke, X.; Hu, H.; Zhang, K.; Xu, W.; Zhu, Q.; Wu, L.; Hu, X. Chem. Commun. 2009(9), 1037-1039.
53. Kozuch, S.; Shaik, S. Accounts of Chemical Research 2011, 44(2), 101-110.
54. Li, X.; Peng, K.; Liu, X.; Xia, Q.; Wang, Y. ChemCatChem 2017, 9(14), 2739-2746.
55. Azizi, N.; Kamrani, P.; Saadat, M. Applied Organometallic Chemistry 2016, 30(6), 431-434.
56. Since the catalytic amount of FeCl2 is soluble in the presence of 2,3-dimthethyloxirane and ethyl amine instead of FeCl2 cluster, single FeCl2 molecule charges are taken into consideration.